Fletcher, T.M. and Duraisamy, K. and Brown, R.E. (2008) *Aeroacoustic analysis of main rotor and tail rotor interaction.* In: 34th European Rotorcraft Forum, Liverpool, England.

http://eprints.gla.ac.uk/4999/

Deposited on: 6 July 2009

Aeroacoustic Analysis of Main Rotor – Tail Rotor Interaction

Timothy M. Fletcher[*]   Karthikeyan Duraisamy[†]   Richard E. Brown[‡]

Rotor Aeromechanics Laboratory
Department of Aerospace Engineering
University of Glasgow
Glasgow, G12 8QQ, United Kingdom

The increased restrictions placed on helicopter noise levels over recent decades have encouraged manufacturers to better understand tail rotor noise and its aerodynamic sources. A generic single main rotor and tail rotor helicopter has been simulated in high speed forward, and quartering, flight using the Vorticity Transport Model. The unsteady loads developed on the tail rotor blades and the resulting acoustic noise propagation have been computed. The sound propagation from isolated tail rotors with top-aft and top-forward senses of rotation in high speed forward flight results in impulsive sound being directed downward from the former and upward from the latter. The principal source of tail rotor noise in high speed forward flight is a periodic blade-vortex interaction between the tail rotor blades. The effect of aerodynamic interaction on tail rotor noise is highly dependent on the flight speed and trajectory, such that the noise produced as a result of interaction is, for the particular helicopter geometry simulated here, greater in quartering flight than in high speed forward flight. The sound pressure produced by periodic impulsive loads in high speed forward flight and the high frequency sound generated in quartering flight is sensitive to the scales to which the vortical features within the wake, and the radial and azimuthal distributions of blade loading, are resolved.

Nomenclature

c	aerofoil chord
C_n	blade loading coefficient, $F_n / \frac{1}{2}\rho c u_b{}^2$
C_T	main rotor thrust coefficient, $T / \rho\pi\Omega^2 R^4$
C_{T_t}	tail rotor thrust coefficient, $T_t / \rho\pi\Omega_t{}^2 R_t^4$
F_n	sectional normal force
M	sectional Mach number
R	main rotor radius
R_t	tail rotor radius
T	main rotor thrust
T_t	tail rotor thrust
u_b	flow velocity relative to the blade
β_{1s}	lateral main rotor disc tilt
β_{1c}	longitudinal main rotor disc tilt
θ_0	main rotor collective pitch
θ_{0_t}	tail rotor collective pitch
θ_{1s}	sine component of main rotor cyclic pitch
θ_{1c}	cosine component of main rotor cyclic pitch
μ	overall advance ratio
ρ	density
ψ	rotor azimuth angle
ω	vorticity
Ω	main rotor rotational speed
Ω_t	tail rotor rotational speed

Abbreviations

BVI	blade-vortex interaction
MR/TR	main rotor – tail rotor
SPL	sound pressure level
VTM	Vorticity Transport Model

Introduction

The regulatory constraints on the sound generated by helicopters are more acute now than at any other time during the seventy year history of helicopter flight. Civilian operations over densely populated conurbations, and military operations which require low observability, have imposed the need for the noise levels associated with helicopter flight to be reduced. Whilst the engines and mechanical drive assembly are, of course, responsible for a significant amount of both the discrete frequency and broadband noise produced by helicopters, a substantial proportion of the sound is generated by the aerodynamic unsteadiness within the system. Helicopters are susceptible to many forms of aerodynamic interaction, the most problematic of which are described in the survey paper by Sheridan and Smith (1). These aerodynamic interactions, which include, for example, the mutual interference between the main rotor wake and fuselage, or the main rotor and tail rotor, can result in significant levels of aerodynamically generated sound.

---

[*]Post-Doctoral Research Assistant, t.fletcher@eng.gla.ac.uk
[†]Lecturer, dkarthik@aero.gla.ac.uk
[‡]Mechan Chair of Engineering, rbrown@aero.gla.ac.uk

The noise generated as a result of main rotor – tail rotor (MR/TR) interaction has received a fluctuating share of research interest over recent decades, however, ambiguity regarding the sources of tail rotor noise persists. In particular, it is not known to what extent aerodynamic interaction is a source of noise in itself. This is in contrast to those sources of noise which would exist if each of the rotors were to be operated in isolation, such as tail rotor blade-to-blade vortex interactions. One of the earliest examples of unacceptable levels of noise developed as a result of main rotor – tail rotor interaction occurred on the Westland Lynx, as reported by Leverton *et al.* (2). Flight tests were performed on the Lynx in its original production configuration in order to isolate the source of the distinctive 'burble' sound produced by the aircraft. The tail rotor on the initial production variants of the Lynx was mounted such that the blades rotated toward the nose of the aircraft at the top of the disc (or top-forward). This arrangement was found to lead to intense pulses of sound at a frequency that correlated with the tail rotor blades crossing through the main rotor tip vortices, which in forward flight would pass close-to or across the tail rotor disc. Similar tests were performed on a modified Lynx with a tail rotor rotating in the top-aft sense and the problematic amplitude and directivity of the radiated sound was alleviated. This discovery was examined in greater detail in a later work by Leverton (3), and led to the Mk. 7 production Lynx being modified with a top-aft tail rotor. Subsequently, during the development of the EH101 Merlin (4), a tail rotor with a top-aft sense of rotation was used and care was taken when selecting the tip speed of the tail rotor blades.

Experimental studies of main rotor – tail rotor interaction noise have been relatively few in number. Schultz and Splettstoesser (5) performed a wind tunnel test on a model Bo 105 helicopter in order to understand the significance of main rotor – tail rotor interaction as a noise source, and to investigate the likely effects of improved tail rotor blade design. It was found that, in contrast to previous studies such as that by Leverton *et al.* (2), in a modest climb the disruption of the tail rotor vortex system by the main rotor wake reduced the impulsive noise associated with tail rotor blade-vortex interactions (BVI). Schultz and Splettstoesser also found that the tail rotor was the dominant source of impulsive noise in climbing and in level forward flight, whereas in descent, the main rotor would generate the largest proportion of noise as a result of more pronounced main rotor BVIs.

The pan-European HeliNOVI project (6,7) was designed in part to build on the work of Schultz and Splettstoesser in order to further investigate the helicopter tail rotor as a noise source and to understand the effect of main rotor – tail rotor interaction. A dynamically and Mach-scaled Bo 105 model was again used with a similar set of test configurations and flight conditions as those investigated by Schultz and Splettstoesser (5). The sensitivity of aerodynamically generated noise to the direction of tail rotor rotation was also investigated. In contrast to the findings of Leverton *et al.* (2), this study indicated that in climbing and in level forward flight, the mean noise level of the

helicopter was lower when the tail rotor had a top-forward sense of rotation. It is possible, however, that the considerably lower position at which the top-forward tail rotor was mounted with respect to the main rotor on the Lynx exacerbated the production of noise as a result of the tail rotor blades intersecting the main rotor tip vortices. Yin *et al.* (6) showed that this result can be explained by the top-forward tail rotor achieving several benefits over a tail rotor with the reverse sense of rotation, including an increased noise source-to-observer distance and a displacement of the advancing blade away from the main rotor tip vortices. Each of these statements suggest that the acoustics of the tail rotor are highly dependent on relatively subtle aspects of the test configuration.

A variety of numerical models have been applied to the analysis of the noise generated by main rotor – tail rotor systems. Tadghighi (8) used a free wake simulation tool, followed by the commonly used acoustic analysis methodology based on the Farassat 1A formulation of the Ffowcs Williams-Hawkings equation (9), to investigate the acoustic pressure associated with tail rotor orthogonal blade-vortex interaction. Good correlation was achieved between the impulse in acoustic pressure associated with the tail rotor blades passing through the main rotor tip vortices, and between the sound pressure level occurring at frequencies in the range 0–3.75kHz sampled at various locations around the rotor. Yin and Ahmed (10) used a free-wake model to investigate the effect of main rotor – tail rotor interaction on tail rotor noise generation. As a result of the work, Yin and Ahmed postulated that the interaction of the main rotor wake with the tail rotor would lead to a significant change in the directivity of tail rotor noise when compared to the noise produced by an equivalent isolated tail rotor.

Numerical models which are capable of simulating the effects of main rotor – tail rotor interaction on the performance of helicopter rotors, and the sensitivity of that performance to the direction of tail rotor rotation are now becoming available (11). In order to design quieter helicopters in the future, it is essential to develop the tools available to designers so that the acoustic implications of aerodynamic interactions on a particular aircraft may be understood. The aim of this paper is show how the characteristics of tail rotor noise and its aerodynamic sources may be better understood by using a methodology which encapsulates the pertinent physics.

Helicopter Aerodynamic Model

The aerodynamics of a generic helicopter with a single main rotor and tail rotor has been simulated using the Vorticity Transport Model (VTM) developed by Brown (12), and extended by Brown and Line (13). The VTM is a comprehensive rotorcraft model in which the flow field around the rotorcraft is computed by solving the time-dependent Navier-Stokes equation, in finite-volume form, on a structured Cartesian mesh enclosing the helicopter system. The key feature of the VTM is its use of the vorticity-velocity

form of the incompressible Navier-Stokes equation,

$$\frac{\partial}{\partial t}\omega + u \cdot \nabla \omega - \omega \cdot \nabla u = S \qquad (1)$$

that relates the evolution of the vorticity field ω, representing the wake, to the velocity field u. The source term

$$S = -\frac{d}{dt}\omega_b + u_b \nabla \cdot \omega_b \qquad (2)$$

accounts for the production of vorticity in the flow as a result of the spatial and temporal changes in the bound vorticity distribution, ω_b, on the various lifting surfaces of the rotorcraft. In the current version of the VTM, the blade aerodynamics is modelled using an extension of the Weissinger-L lifting-line theory (14). The velocity field is related to the vorticity field by using a Cartesian fast multipole method to invert the differential form of the Biot-Savart law

$$\nabla^2 u = -\nabla \times \omega . \qquad (3)$$

Use of the fast multipole method in conjunction with the adaptive grid renders the approach effectively boundary free (13). The computational efficiency of the method is further improved by using an adaptive grid formulation in which cells only exist where there is vorticity. Numerical diffusion of the vorticity in the flow field surrounding the rotorcraft is kept at a very low level by using a technique based on Toro's weighted average flux method (15) to advance Eq. (1) through time. This approach allows highly efficient multi-rotor simulations, and permits many rotor revolutions to be captured without significant dissipation of the wake structure, in contrast to the performance of more conventional CFD techniques based on the pressure-velocity formulation of the Navier-Stokes equations.

In this study, the helicopter is represented as a pair of rotors, oriented in a conventional fashion with their centres located at representative points in the flow. This idealisation of the problem ensures that solely the effects of the interactions between the rotors are captured, uncomplicated by the presence of further aerodynamic interactions between rotors and fuselage or empennage. The principal parameters for the main and tail rotors are given in Table 1. The main rotor rotates anti-clockwise when viewed from above (the convention for American helicopters), hence the tail rotor produces a force to starboard in trimmed flight. The tail rotor is of a two-bladed teetering design, whilst the main rotor is articulated and all blades are modelled as rigid. The rotor thrust coefficients and main rotor disc tilt angles were selected, where possible, to be similar to those used during the HeliNOVI tests (6), and these values, along with the rotor control angles in trimmed flight conditions, are listed in Table 2.

In the present work, two flight trajectories have been used to investigate the sources of tail rotor noise: forward flight at an advance ratio of 0.275 and rearward quartering flight at an advance ratio of 0.04 along a bearing of 225° from nose-forward, as illustrated by Fig. 1. Forward flight was chosen as it provides an excellent benchmark case on which several previous studies have been based, and where

Table 1: Rotor Data

	Main Rotor	Tail Rotor
No. of blades	4	2
Rotor radius	R	$R_t = 0.1915R$
Chord	$0.0605R$	$0.1932R_t$
Twist	$-8°$ (linear)	$0°$
Aerofoil	NACA 23012	NACA 0012
Root cut-out	$0.22R$	$0.4178R_t$
Rotational speed	Ω	$\Omega_t = 5\Omega$

Table 2: Trim Data

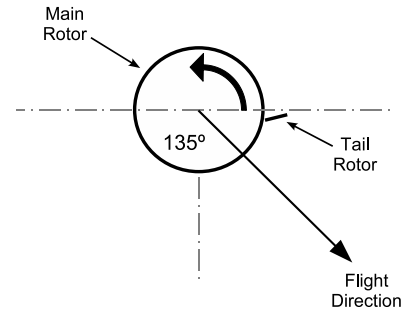|	Forward Flight	Quartering Flight
C_T	0.0052	0.0052
C_{T_t}	0.00545	0.00507
θ_0	6.5°	7.9°
θ_{0_t}	7.1°	8°
θ_{1s}	−1.6°	1.5°
θ_{1c}	0°	−0.6°
β_{1s}	0°	0°
β_{1c}	−3°	0°

Figure 1: *Quartering flight trajectory.*

some of the aerodynamic causes of tail rotor noise are relatively well known. Aerodynamic interaction between the main and tail rotors of a conventional helicopter is known to be considerable in low speed quartering flight (11), and this flight condition is therefore ideal to illustrate and better understand the effect of main rotor – tail rotor interaction on the generation of noise by tail rotors.

Acoustic Methodology

The acoustic field of the rotor system is determined using the Farassat 1A formulation of the Ffowcs Williams-Hawkings equation (9). The instantaneous acoustic pressure, $p_L(t)$, at a given observer location due to a discrete point force, F, moving at Mach number M, is given by

$$p_L(t) = \frac{1}{4\pi a_0}\left[\frac{\partial}{\partial t}\left(\frac{F_\tau}{r(1-M_\tau)}\right) + \frac{a_0 F_\tau}{r^2(1-M_\tau)}\right]_\tau \qquad (4)$$
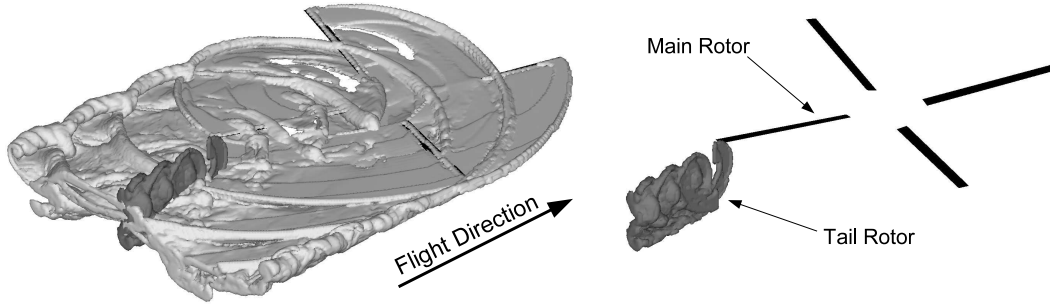
Figure 2: *Wake of the main rotor – tail rotor system in forward flight at an advance ratio of 0.275. Left: main (light contour) and tail rotor wakes. Right: relative location of the tail rotor wake to the main rotor.*

where a_0 is the speed of sound, and r is the distance between the observer and the source. The term in the square bracket is evaluated at the source time τ at which the sound was emitted. Since the blade surface in the aerodynamic model is represented by a series of panels, the force contributed by each panel is treated as a point source located at the collocation point of the panel. The noise produced by these sources is then propagated according to Eq. (4). The aerodynamic effects of blade thickness are introduced through a look-up table of aerofoil characteristics, but the lifting-line model within the VTM otherwise assumes an infinitesimally thin blade. The thickness noise is thus modelled independently using a source-sink pair attached to each panel along the length of the blades. Noise due to quadrupole terms is neglected in the present work. The coupled VTM-acoustics methodology has been used previously to predict the acoustics of the HART II rotor (16), where good agreement between the computed pressure time-histories and sound pressure levels was demonstrated against experimentally measured data in three representative flight conditions involving strong BVIs.

Figure 3: *Tail rotor blade loading coefficient (C_nM^2) at the $0.8R_t$ radial location in forward flight at an advance ratio of 0.275.*

Aerodynamic Effects of Main Rotor – Tail Rotor Interaction

The aerodynamic interaction between the main and tail rotors of a conventional helicopter results in a mutual, but not equal, effect on the performance of both rotors. The degree of unsteadiness imparted into the performance of each of the rotors is a strong function of the helicopter geometry and the flight condition, with the unsteadiness in low speed quartering flight having a larger effect on the performance of both the main and tail rotors than in high speed forward flight (11). In general, the performance of the tail rotor is more largely affected by main rotor – tail rotor interaction than the performance of the main rotor. This imbalance is caused, in part, by the relative areas of the main and tail rotor discs, and by the fact that the interaction between the rotors manifests as a large-scale distortion of the wake in the region between the two rotors. Additionally, the performance of the tail rotor in a combined MR/TR system is sensitive to the direction of rotation of the tail rotor with respect to the main rotor (17).
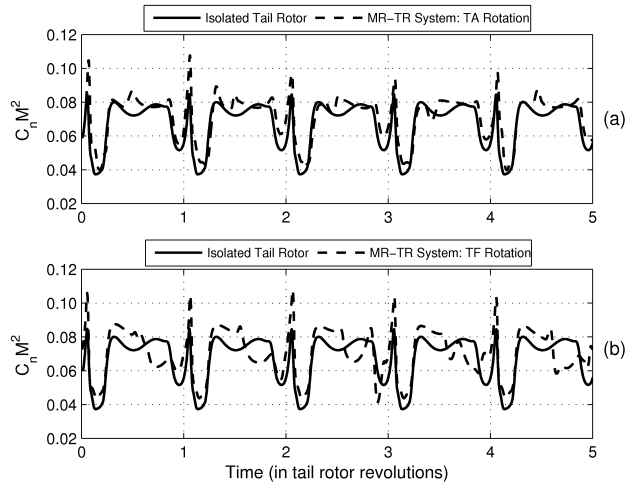
Figure 2 illustrates the general features of the wake of a MR/TR system in forward flight at an advance ratio of 0.275. The image on the left of Fig. 2 shows the main and tail rotor wakes rendered as surfaces of constant vorticity magnitude, whilst on the right, the main rotor wake has been omitted in order to illustrate the relative position of the tail rotor and its wake with respect to the main rotor. In the figure, each of wakes has been rendered separately, with the tail rotor wake represented using the darker colour. In forward flight at a relatively high advance ratio, the combined wake of the MR/TR system is almost identical to the epicycloidal form of the wake of an isolated main rotor operating at the same flight condition. In addition to the wake structure induced by an isolated main rotor, a compact, spine of vorticity is induced by the tail rotor which propagates along the centreline of the overall wake between the periphery in which the main rotor tip vortices coalesce. The downstream convection of the main and tail rotor wakes downstream ensures that the influence of the tail rotor wake on the performance of the main rotor is restricted to very subtle changes in loading at the rear of the main rotor disc (around $\psi = 0°$).
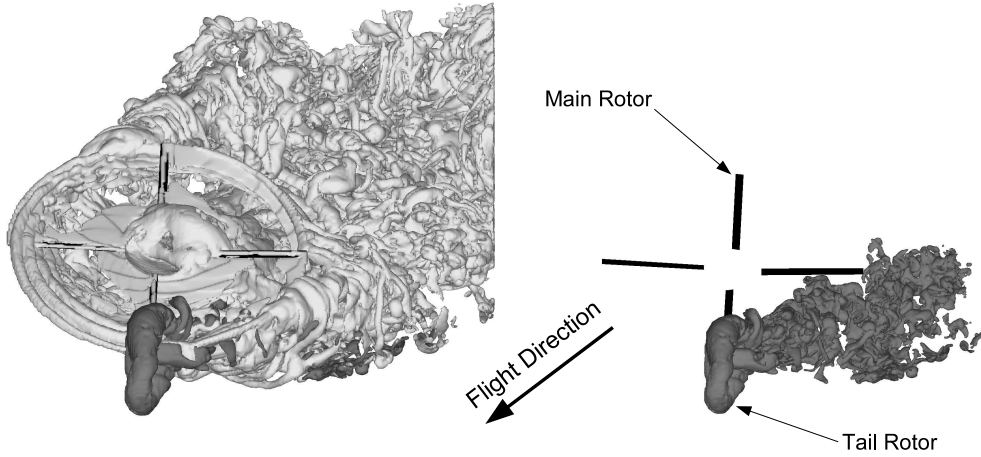
4

Figure 4: *Wake of a main rotor – tail rotor system in quartering flight at an advance ratio of 0.04. Left: main (light contour) and tail rotor wakes. Right: relative location of the tail rotor wake to the main rotor.*

In high speed forward flight, the tail rotor blades are subject to a large impulsive load arising from a vortex interaction between each blade and the trailed vortex of the preceding blade. The blade loading, C_nM^2, sampled at a radial station of $0.8R_t$, for an isolated tail rotor, and for top-aft and top-forward tail rotor configurations operating as part of a MR/TR system in high speed forward flight is shown in Fig. 3. The impulsive loading associated with the tail rotor self-BVI is unchanged in azimuthal location for each of the three configurations that are represented. The amplitude of the loading during the impulse does, however, vary between the three cases. A comparison of the isolated and top-aft tail rotor cases in Fig. 3(a) illustrates how the operation of the tail rotor in close proximity to the main rotor increases the amplitude of the impulsive loading associated with tail rotor self-BVI. Figure 3(b) shows that a similar increase in impulsive loading occurs on the tail rotor with a top-forward sense of rotation. At azimuthal locations between those at which the blade loading is dominated by the effect of the self-BVI, the loading is subtly more unsteady when the tail rotor is combined with a main rotor, and is sensitive to the direction of tail rotor rotation. This increased unsteadiness is caused by the modification of the velocity field in which the tail rotor operates as a result of its partial immersion within the main rotor wake.

In contrast to the high speed forward flight condition, the interaction between the main and tail rotors in quartering flight, at a low advance ratio of 0.04, is substantial. With reference to Fig. 4, it is clear that the tail rotor wake passes largely through the main rotor disc, and is entrained into the wake of the main rotor. Note that the main and tail rotor wakes are represented in Fig. 4 using the same conventions as those used in Fig. 2. The wake induced by the MR/TR system demonstrates little of the structure that is evident in high speed forward flight, and the development of vortex instabilities results in both rotors operating in a substantially more unsteady environment than is the case in high speed forward flight.

The loading on the blades of tail rotors with both top-aft and top-forward senses of rotation is modified significantly
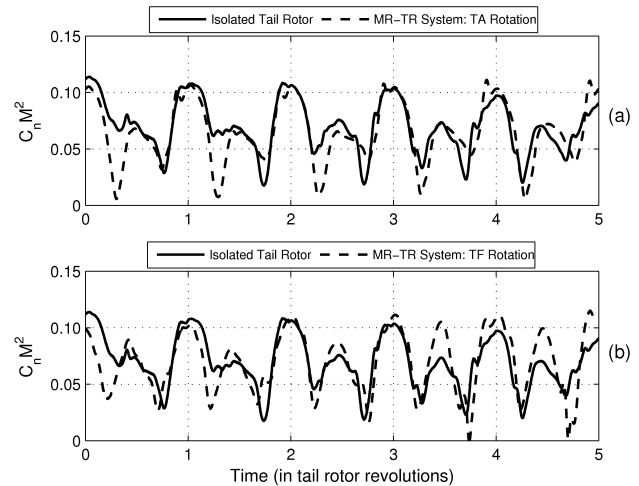

Figure 5: *Tail rotor blade loading coefficient (C_nM^2) at the $0.8R_t$ radial location in quartering flight at an advance ratio of 0.04.*

as a result of aerodynamic interaction in quartering flight. By comparing the blade loading at $0.8R_t$ for the three tail rotor configurations, as shown in Fig. 5, it is evident that, in general, the correlation between the loading on the top-aft and top-forward tail rotor blades with that on the isolated tail rotor blades is relatively good on the advancing side of the tail rotor disc, as illustrated by the loading between times 0.5 and 1 in Figs. 5(a) and (b). The loading on the retreating side of the tail rotor disc demonstrates the significant effect of aerodynamic interaction between the main and tail rotors, as the impulsiveness of the loading on both the top-aft and top-forward tail rotors is increased relative to the isolated tail rotor. It should be noted, however, that recurrence in the loading on the tail rotor blades over the duration of several rotor revolutions is limited by aperiodic fluctuations in the size and strength of the larger vortical structures around the tail rotor. This effect is particularly clear in the loading on the blades of the isolated tail rotor shown in Fig. 5.
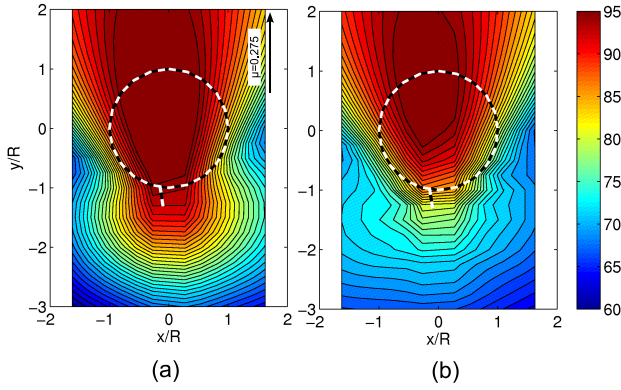
Figure 6: *Sound pressure level generated as a result of blade thickness effects by tail rotors with top-aft (left) and top-forward (right) senses of rotation in forward flight at an advance ratio of 0.275 (relative location of main and tail rotors is shown for clarity).*

Sound Pressure Characteristics

A comparison of the thickness noise produced by tail rotors with top-aft and top-forward senses of rotation operating in forward flight in conjunction with a main rotor is shown in Fig. 6. The contours of sound pressure level (SPL) shown in the figure have been calculated at an array of observer locations on a horizontal plane located at a distance of 1.15R beneath the rotor system. As expected, the amplitude and directivity of the thickness noise produced by the tail rotor is largely insensitive to its direction of rotation and is, by definition, unaffected by aerodynamic interaction between the main and tail rotors. The region in which the thickness noise is highest is located approximately along a plane that is coincident with the tip path plane of the tail rotor, as would be expected since the displacement of fluid due to the thickness of the blades is greatest in the plane of the rotor. The small differences in thickness noise shown by a comparison of Figs. 6(a) and 6(b) are due to differences in the retarded time caused by the reversal of the sense of tail rotor rotation. Importantly, with the exception of the concentrated region ahead of the main rotor, the amplitude of the thickness noise is considerably lower than that due to the loading on the blades. As a result, the thickness noise component has been omitted from all analysis beyond this point, thus facilitating the understanding of tail rotor loading noise and its aerodynamic sources.

The component of the overall SPL produced as a result of the loading on the tail rotor blade for the system in both forward and quartering flight, and when the tail rotor is operated in isolation and in a MR/TR system with both top-aft and top-forward senses of rotation, is shown in Figs. 7 and 8. When generating each of the contour maps shown in Figs. 7 and 8, only the sound pressure signal contribution occurring at frequencies in the range 5–40-per-tail rotor revolution has been shown in order to emphasise the impulsive noise that is generated as a result of aerodynamic interactions, which would otherwise be masked by noise occurring at lower frequencies. In forward flight at an advance ratio of 0.275, a tail rotor with a top-aft sense of rotation operated in isolation generates a distinct concentration of sound pressure on either side of the tail rotor; the higher of the two being located on the port side, as shown in Fig. 7(a). A similar distribution of sound pressure was also evident during the HeliNOVI tests performed on an isolated tail rotor with top-aft rotation in a very similar flight condition (6). In contrast, the sound pressure generated by the isolated top-forward tail rotor has a considerably different directivity to that of the top-aft tail rotor, as shown by a comparison of Figs. 7(a) and 7(c). The region of highest sound pressure lies ahead of the tail rotor, rather than to either side. When both tail rotor configurations are combined with a main rotor in forward flight, the effect on the noise produced by the tail rotor is very small, with only subtle changes in amplitude in the regions of most intense sound pressure, as shown in Figs. 7(b) and 7(d).

Figures 8(a)–8(c) show the sound pressure on the same plane beneath the rotor system in quartering flight. In the quartering flight condition simulated here, the component of lateral velocity places the tail rotor in effective descent, and as a result both the aerodynamic performance of the tail rotor and the loading noise that it generates differ substantially from that in high speed forward flight. An examination of Fig. 8(a) shows that the point of highest loading noise on the observer plane for the isolated top-aft tail rotor is located to the port side of the rotor, and has an amplitude similar to the maximum SPL due to blade loading found for an equivalent tail rotor in forward flight, as shown in Fig. 7(a).

The influence of main rotor – tail rotor interaction on the performance of each of the rotors is distinctly more global in quartering flight than in high speed forward flight. A comparison of Figs. 8(a) and 8(b) shows that when the top-aft tail rotor is combined with the main rotor, the region of highest loading noise is far more concentrated than in the case of the isolated rotor. An examination of Fig. 8(c) shows that large areas of elevated loading noise occur on either side of the top-forward tail rotor, in contrast to the acoustic signature of the top-aft tail rotor shown in Fig. 8(b).

Influence of Tail Rotor Sense of Rotation on Sound Propagation

The considerable differences in the directivity of the loading noise that is evident between Figs. 7(b) and 7(d), and between Figs. 8(b) and 8(c), suggest that there is a high sensitivity in the propagation of loading noise from the tail rotor blades to the sense in which the tail rotor rotates. Figure 9 shows the loading SPL on a spherical observer surface of radius 2.5R around an isolated tail rotor operating in high speed forward flight. In Fig. 9(a), the tail rotor rotates in the top-aft sense with respect to the flight direction, whilst in Fig. 9(b), the tail rotor rotates in the top-forward sense. In order to understand better the directivity, consider a section of the tail rotor blade translating through the fluid
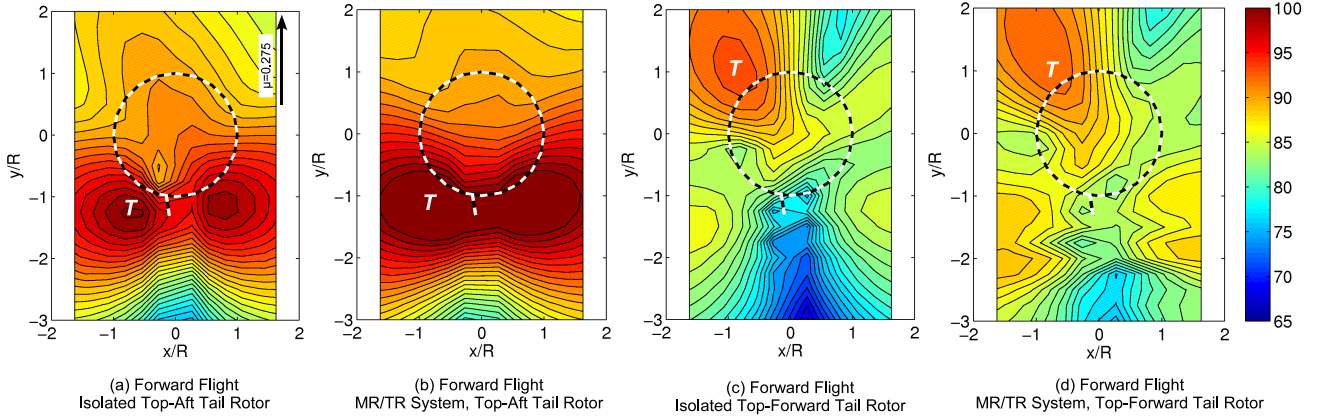
6

Figure 7: *Tail rotor loading SPL (5–40/rev) in decibels for four different rotor systems in forward flight at an advance ratio of 0.275 (relative location of main and tail rotors is shown for clarity).*
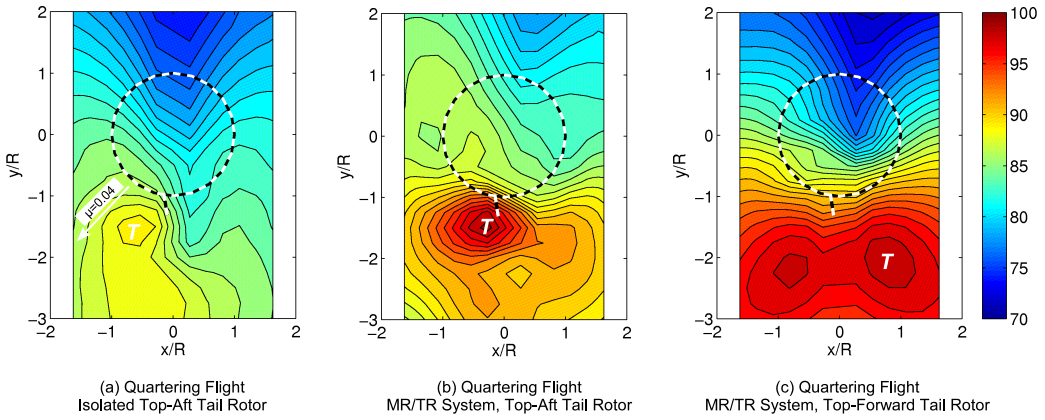

Figure 8: *Tail rotor loading SPL (5–40/rev) in decibels for three different rotor systems in quartering flight at an advance ratio of 0.04 (relative location of main and tail rotors is shown for clarity).*

at a local Mach number, M, whilst generating a local force $F(t)$. The far-field noise at an observer located at a distance r from the source can be shown to be approximately proportional to

$$\frac{1}{r} \left(\frac{dF}{dt} \cdot \hat{r} \right) \left[\frac{1}{(1 - M \cdot \hat{r})^2} \right], \qquad (5)$$

where, $\hat{r}$ is the normalised position vector between the observer and the point of application of F. Note that all the quantities are evaluated in retarded time. The $1/r$ term represents the decay of the noise with increasing distance (and is approximately constant on the sphere), and dF/dt is the noise source due to the unsteadiness in the aerodynamic force. The term $(dF/dt) \cdot \hat{r}$ will thus be of maximum magnitude within two conical regions on either side of the tail rotor disc (since $F(t)$ is predominantly normal to the tail rotor plane). The Doppler term in the square brackets acts to selectively intensify or diminish the aforementioned noise sources on the disc, and thus plays a major role in determining the focus of the noise.

The cones of intense loading noise produced by the top-aft tail rotor are directed toward the ground on either side

of the rotor, as can be seen in Fig. 7(a). In contrast, when the sense of rotation is reversed, these focused regions are directed away from the ground. While a degree of reflectional symmetry can be expected on an observer sphere which is located at a fixed position with respect to the rotor system, such a distinct change in the directivity of the noise is of high practical significance. In addition to these noise maxima, a third region of elevated sound pressure is noticeable toward the front of the rotor as can be seen in Fig. 7(c). This region is narrow and is shaped entirely by the high rate of Doppler amplification of the noise sources on the advancing side of the rotor. For the top-forward configuration, this region is oriented more toward the ground in contrast to the top-aft case. Alternately, the diminishing effect of the Doppler terms acts to generate a narrow region of low noise toward the rear of the aircraft as seen for both top-aft and top-forward tail rotor configurations in Fig. 9.

Noise Sources

Past research into tail rotor noise has collectively set forward various explanations for its aerodynamic origins. Al-
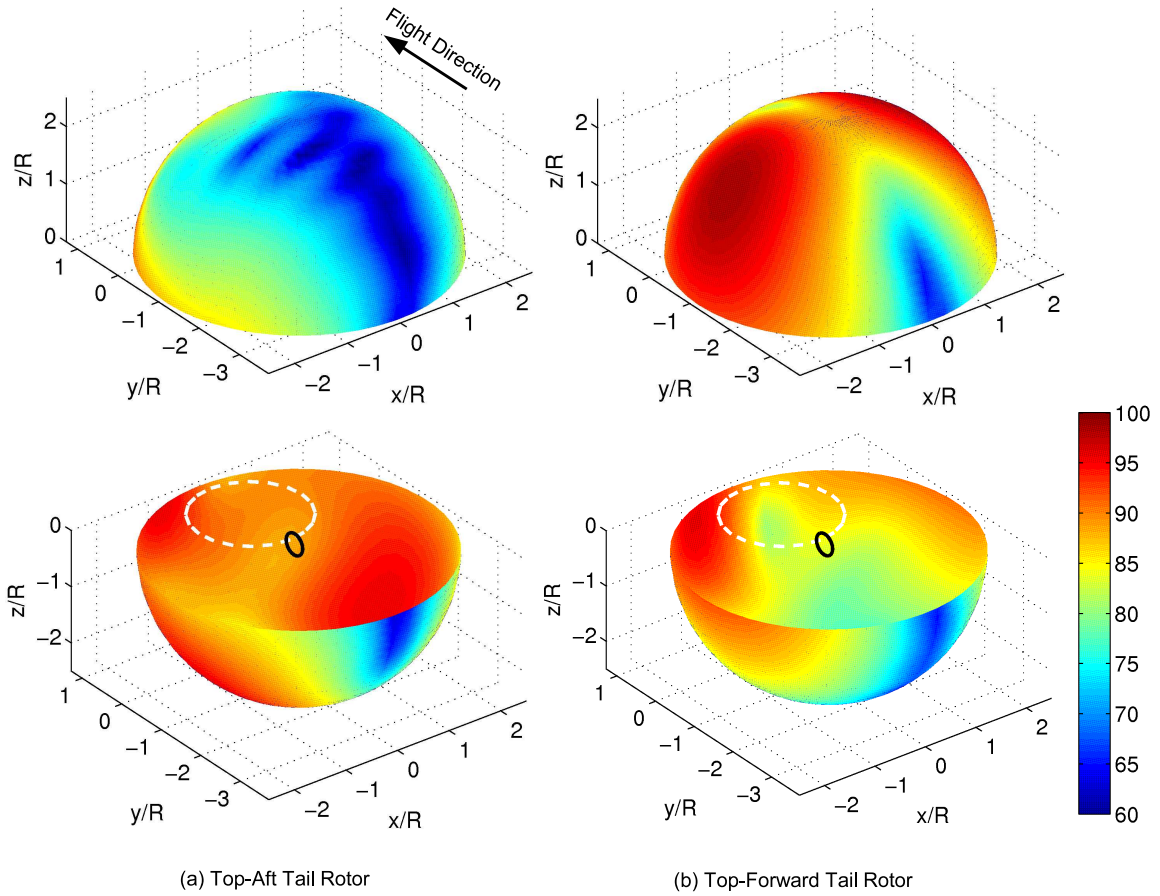
7

(a) Top-Aft Tail Rotor   (b) Top-Forward Tail Rotor

Figure 9: *Sound pressure level due to loading in decibels on a spherical observer surface 2.5R from isolated tail rotors with both top-aft and top-forward senses of rotation in forward flight at an advance ratio of 0.275.*

though it is abundantly clear that the propagation of sound from conventional helicopters is a strong function of the flight trajectory and geometry of the aircraft, the principal acoustic signature of the tail rotor originates from very specific aerodynamic effects. The principal effects are tail rotor self-BVIs, orthogonal tail rotor interaction with main rotor tip vortices, and whether indeed the immersion of the tail rotor within the main rotor wake may actually reduce the noise generated by tail rotor, as suggested in the past (5). The aim of this section is to understand better these relationships, both in the case of high speed forward flight, and in the rather more aperiodic and therefore less straightforward case of low speed quartering flight.

Figures 10 and 11 show the loading component of the overall sound pressure produced over the duration of 5 rotor revolutions by a tail rotor operating in forward flight and in quartering flight, respectively, in each of the configurations described previously and represented in Figs. 7 and 8. In each of the cases shown in Figs. 10 and 11, the sound pressure has been calculated at the point of maximum SPL (labelled '*T*') on the corresponding observer plane shown in Fig. 7 or 8.

In forward flight, the loading noise produced by the tail rotor in each of the four configurations represented in Fig. 10 is qualitatively very similar, with the principal feature being a two-per-rev (2/rev) impulsive sound.

The peak-to-peak amplitude of the impulse varies between the four configurations, with the top-aft tail rotor in a MR/TR system generating an impulse in sound pressure of considerably greater amplitude than the equivalent top-forward tail rotor, as shown by a comparison of Figs. 10(b) and 10(d). Indeed, the loading noise generated by the top-forward tail rotor is considerably less impulsive than that of the tail rotor with a top-aft sense of rotation, and emerges more gradually over approximately 90° of tail rotor azimuth. The fact that the impulse is present in the acoustic signature from both the isolated top-aft tail rotor and the top-aft tail rotor operating in conjunction with a main rotor implies that the aerodynamic origin of this impulse is a blade-vortex interaction between each blade and the tip vortex which evolves behind the preceding blade of the same rotor. The tail rotor self-BVI in question is clearly illustrated in Fig. 12, in which the lower of the two blades (rendered in black) passes within one blade chord of the tip vortex generated by the preceding tail rotor blade. The differences in impulsive loading noise that are evident between each of the configurations represented in Fig. 10 demonstrate that the loading on the tail rotor blades is sensitive to interaction between the main and tail rotors, but that its contribution to the loading noise developed by the tail rotor is lower than that generated by self-BVIs.

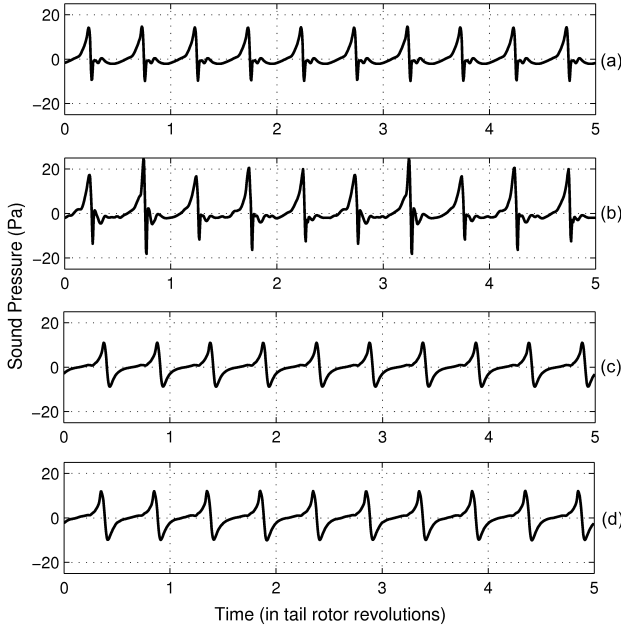The sound pressure at the point of maximum loading

Figure 10: *Sound pressure due to loading generated in forward flight at an advance ratio of 0.275 by tail rotors in the following configurations: isolated top-aft tail rotor (a), MR/TR system with top-aft tail rotor (b), isolated top-forward tail rotor (c), and MR/TR system with top-forward tail rotor (d).*
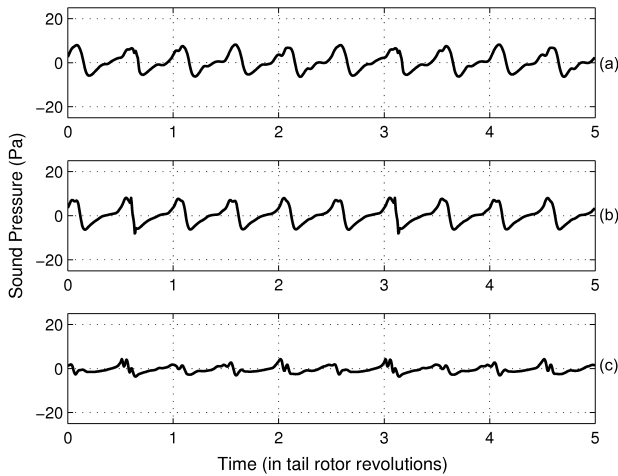

Figure 11: *Sound pressure due to loading generated by tail rotors in isolated (a), top-aft (b) and top-forward (c) configurations in quartering flight; μ = 0.04.*

noise, caused by changes in loading on the tail rotor blades, has a somewhat different character in quartering flight when compared to the high speed forward flight cases. Figures 11(a) to 11(c) show that the loading noise is considerably less impulsive than in forward flight and is primarily composed of a 2/rev variation in sound pressure corresponding to the tail rotor blade passage frequency. The sound pressure at the location of maximum loading noise is very similar in tone and amplitude for the isolated tail rotor
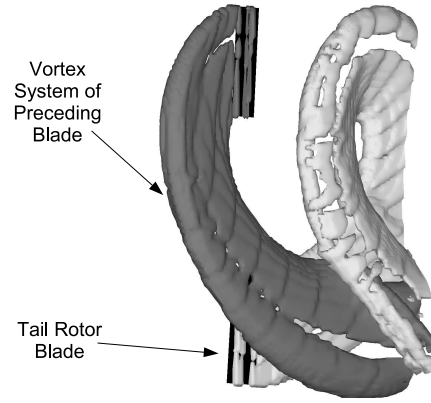

Figure 12: *Illustration of a tail rotor blade-vortex interaction in forward flight at an advance ratio of 0.275.*

(with top-aft sense of rotation) and the top-aft tail rotor operating in a MR/TR system, as can be seen by comparing Figs. 11(a) and 11(b). When the sense of rotation of the tail rotor is reversed, however, the amplitude of the 2/rev fluctuations in sound pressure is reduced considerably as shown in Fig. 11(c).

Figure 13 shows the location of the acoustic sources on the tail rotor disc for an isolated tail rotor, for top-aft and top-forward tail rotors operating in a MR/TR system in high speed forward, and in low speed quartering flight. In each of the contour plots shown in Fig. 13, the sources of far-field loading noise have been approximated as the azimuthal and radial variations in the derivative $\partial(C_{n_x}M^2)/\partial\psi$, where $C_{n_x}M^2$ is the component of the blade loading coefficient normal to the tail rotor disc. This derivative is an approximation to the acoustic source term dF/dt in Eq. (5).

There are two primary sources of loading noise on the isolated tail rotor when it operates in high speed forward flight: the blade-vortex interaction which occurs between $\psi = 0°$ and $\psi = 45°$, and the increase in loading which occurs on the advancing side of the tail rotor at $\psi \approx 90°$, as shown in Fig. 13(a). Whilst the derivative $\partial(C_{n_x}M^2)/\partial\psi$ is of similar magnitude at the location of the self-BVI and on the advancing side of the rotor, the increase in loading on the tail rotor blades caused by the self-BVI is rather more impulsive than is the case for the increase in loading on an advancing blade. Figure 13(b) shows that very similar sources of loading noise exist on the tail rotor with a top-aft sense of rotation operating in proximity to a main rotor as are present on the isolated rotor. When the sense of rotation of the tail rotor in the MR/TR system is reversed, the same two principal loading noise sources occur. However, the peak magnitude of the azimuthal change in loading is notably higher than is the case for the isolated and top-aft tail rotors, as shown in Fig. 13(c).

The changes in loading on the tail rotor configurations shown in Figs. 13(d) to 13(f) are caused by a combination of the asymmetry in dynamic head on either side of the rotor disc and the partial immersion of the tail rotor blades within the flow field that is induced by the main
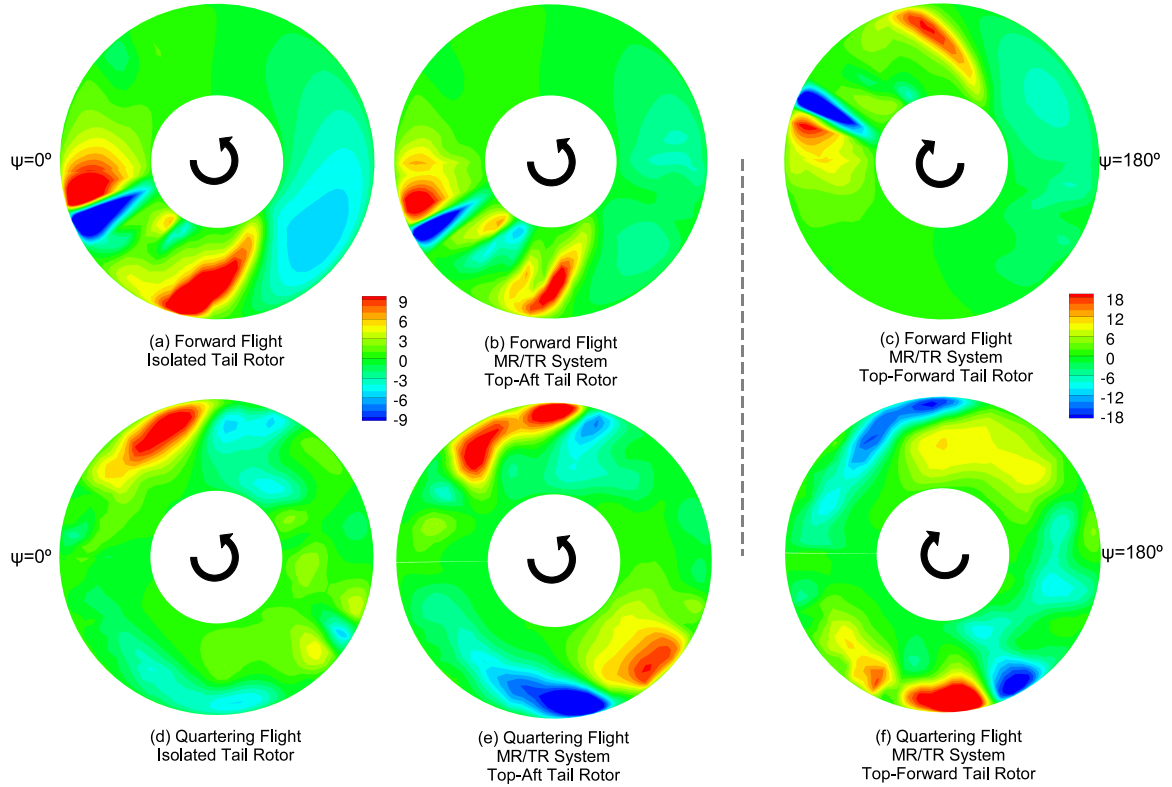
Figure 13: *Acoustic sources, represented by $\partial(C_{n_x}M^2)/\partial\psi$, on three tail rotor configurations in forward flight at $\mu = 0.275$ and quartering flight at $\mu = 0.04$ (shown for the first revolution).*

rotor. The low speed at which the rotor system translates along the quartering trajectory ($\mu = 0.04$) results in only a small asymmetry in tail rotor loading. The low translational speed, however, means that the main rotor wake advects in a mode more closely resembling that of a hovering rotor than the flattened form of a rotor operating in modest or high speed forward flight. The effect of the tail rotor blades operating within the induced flow of the main rotor wake is clearly evident at an azimuth angle of approximately $135°$ in Fig. 13(e) and at approximately $225°$ in Fig. 13(f), where there are significant increases and decreases in loading respectively compared to that of the isolated tail rotor. The increase in loading that is evident at an azimuth of approximately $135°$ in Fig. 13(e) arises because of the increase in dynamic head associated with the tail rotor blade passing through the induced flow of the main rotor; at an azimuth of approximately $225°$ for the top-forward tail rotor, simply the reverse effect occurs. The sources of loading noise in low speed quartering flight are almost entirely the result of main rotor – tail rotor interaction, in direct contrast to the case in high speed forward flight, in which the largest source of loading noise is the blade-vortex interaction which occurs between the tail rotor blades.

Aeroacoustic Sensitivity to Blade and Wake Discretisation

The sound pressure generated as a result of blade loading is dependent on the derivative $\partial(C_nM^2)/\partial\psi$, and is therefore sensitive to the resolution of the aerodynamically-induced loads on the blades. The VTM provides considerable flexibility in the selection of both the density of cells within the computational grid, or wake, and the number of aerodynamic control points used along the blades. The tail rotor thrust coefficient is largely insensitive to the form of discretisation used, however the azimuthal and radial gradients in loading on the blades can change considerably when vortical features within the wake, and the distribution of aerodynamic loading on the blades, are resolved to finer scales. Figure 14 shows a comparison of the SPL due to blade loading generated at an observer located at the maximum noise point on the two-dimensional observer plane used previously. Two different levels of discretisation have been used for the simulation of an isolated tail rotor in both forward and quartering flight conditions. The black line represents the sound pressure computed on a grid with a density of 80 cells per main rotor radius and using 20 aerodynamic control points along the tail rotor blade. In comparison, the grey line represents the sound pressure computed on a grid with a density of 320 cells per main rotor radius and using 32 aerodynamic control points along the tail rotor blade. It is clear from Fig. 14(a) that the
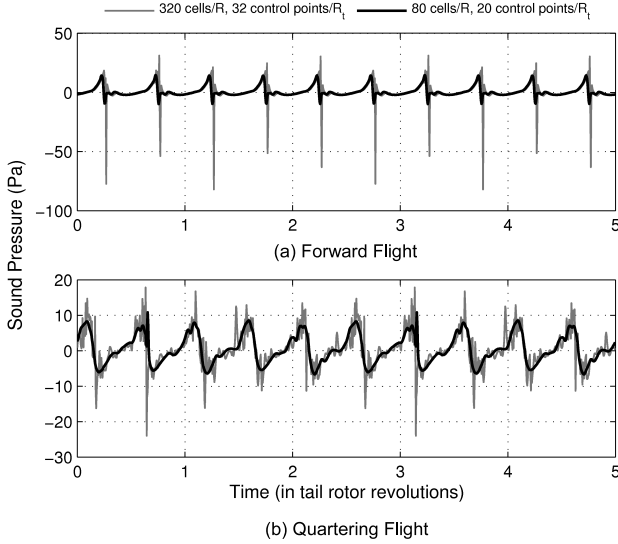
Figure 14: *Sensitivity of loading sound pressure to wake and blade aerodynamic discretisation for an isolated tail rotor in forward and quartering flight, μ = 0.275 and 0.04 respectively.*

Figure 15: *Acoustic sources, represented by components of $\partial(C_n M^2)/\partial \psi$, as a function of blade and wake discretisation in forward and quartering flight at μ = 0.275 and μ = 0.04 respectively. Left: simulated using 80 cells/R, 20 control points/R_t; Right: simulated using 320 cells/R, 32 control points/R_t.*

peak-to-peak amplitude of the impulsive sound associated with tail rotor blade-vortex interaction is predicted to be approximately three times larger by the higher resolution simulation than by the low resolution simulation.

A comparison of the acoustic sources computed for the isolated tail rotor in both forward and quartering flight, for each of the two discretisations described above, is shown in Fig. 15. A comparison of Fig. 15(a) with Fig. 15(b), and Fig. 15(c) with Fig. 15(d), shows that abrupt changes in the derivative of the normal (*x*) and vertical (*z*) components of blade loading occur between $\psi = 0°$ and $\psi = 45°$ when computed using the finer of the two discretisations described above. In contrast, when the coarser discretisation is used, the changes in the blade loading as a result of the BVI are more spatially diffused, and result in a reduction in the impulsive noise generated by the blades, as shown in Fig. 14(a). Indeed, the changes in the vertical component of the blade loading as a result of the tail rotor self-BVI are not captured at all when the rotor is simulated in forward flight at the lower of the two resolutions.

If the same comparison is made between the results of the simulations using the two different discretisations described above for an isolated tail rotor in quartering flight, the principal effect of increasing the resolution is to predict a much larger proportion of loading noise occurring at frequencies substantially above the tail rotor blade passage frequency, as shown in Fig. 14(b). Figure 14(b) shows clearly, however, that the loading sound pressure computed using the lower resolution provides a very good approximation to the sound produced by the loading on the tail rotor simulated at the higher of the two resolutions defined previously, and furthermore demonstrates the convergence of the aerodynamic and acoustic methodologies in the low and moderate frequency bands.
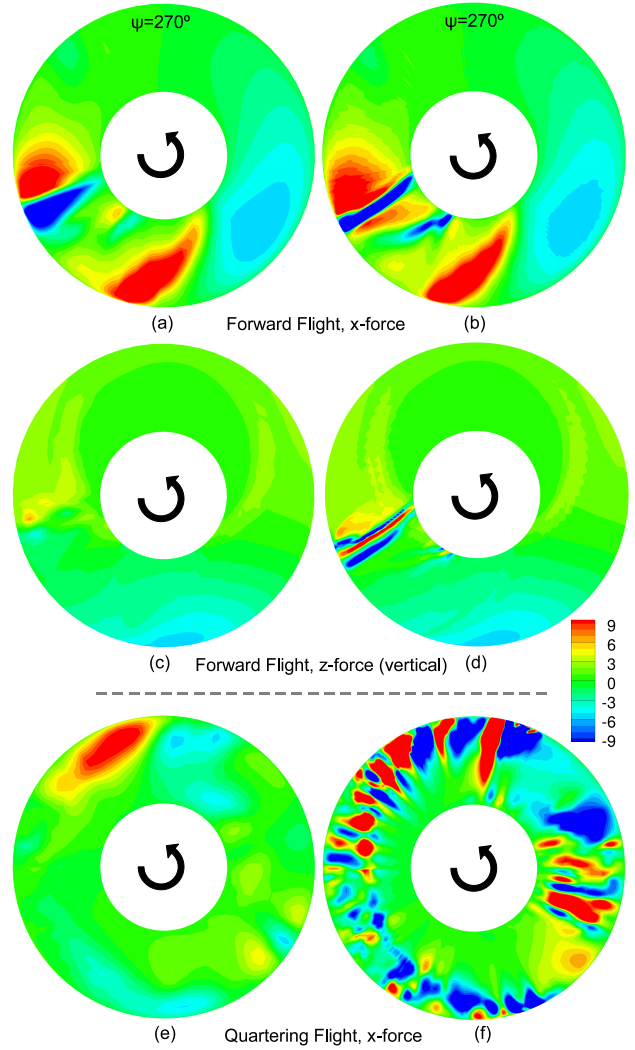
The source of the high frequency loading noise in quartering flight shown in Fig. 14(b) can be understood by comparing Figs. 15(e) and 15(f). When the finer form of discretisation is used, the loading on the tail rotor blades changes both more frequently and more abruptly around the rotor azimuth than is the case when the same rotor is simulated using the coarser discretisation. The gradients of blade loading vary significantly over relatively small azimuthal distances, and therefore result in the radiation of high frequency noise. When an isolated tail rotor is simulated at the lower of the two resolutions, the high frequency variations in blade loading are not present, instead, only 2/rev variations in loading, which represent the mean acoustic sources on the tail rotor, are captured, as shown in Fig. 15(e).

Figure 16: *Wake of an isolated tail rotor in quartering flight at an advance ratio of 0.04. Top: simulated using 320 cells/R, 32 control points/R_t. Bottom: simulated using 80 cells/R, 20 control points/R_t.*

The unsteadiness evident in the blade loading on the tail rotor disc in Fig. 15(f) emerges as a result of the vortical structures within the tail rotor wake being resolved to finer scales. In low speed quartering flight, the tail rotor operates effectively in low speed descent; a condition in which the wake surrounding the rotor is known to manifest as an unsteady toroidal form (11). Figures 16(a) and 16(b) show the wake surrounding an isolated tail rotor in quartering flight computed using the two forms of blade and wake discretisation described previously. In each of the figures, the wakes induced by each of the two blades on the tail rotor have been rendered in different colours, thus allowing the evolution of individual vortex filaments to be more readily observed. Figure 16(a) shows how a large number of vortex filaments trailed from each of the two blades adopt an interleaving pattern as they loop around the tail rotor blades to form a relatively coherent toroid. This flow structure leads to rapidly changing induced velocities at the tail rotor blades as they rotate around the disc, and consequently, in large variations in blade loading. A comparison of Fig. 16(a) with Fig. 16(b) shows that although the toroidal form is still present, the vortical structures surrounding the tail rotor are resolved significantly more coarsely, and therefore cannot impart the same changes to the loading on the tail rotors that occurs over small azimuthal distances, and as demonstrated in Fig. 15(f).

Conclusion

The sound generated by tail rotors with both top-aft and top-forward senses of rotation in high speed forward flight and low speed quartering flight has been investigated using the Vorticity Transport Model and an acoustic methodology based on the Farassat 1A formulation of the Ffowcs Williams-Hawkings equation. Isolated tail rotor and main rotor – tail rotor systems have been simulated in order to better understand the propagation of tail rotor noise and its aerodynamic sources.

The characteristic sound pressure distribution on a two-dimensional observer plane beneath the rotor system is highly dependent on the flight condition and the sense of tail rotor rotation. The directivity of the loading noise generated by the tail rotor in high speed forward flight is largely dependent on the Doppler amplification of the noise generated at particular locations on the tail rotor disc. In low speed quartering flight, the aerodynamic interaction between the main and tail rotors has a considerably larger effect on the performance of the tail rotor than is the case in high speed forward flight. As a result, the directivity of sound pressure that is induced by the sense of tail rotor rotation, and the impulsive loading from which it originates, is, to a large extent, distorted by the interaction between the main and tail rotors.

The principal source of tail rotor noise in high speed forward flight is a parallel blade-vortex interaction between the tail rotor blades and their own wake. In quartering flight, the tail rotor blades pass partially through the flow that is induced by the main rotor. In addition, the tail rotor operates in effective descent where the flow field around the tail rotor is highly disordered and aperiodic, with the result that the distinctive blade-vortex interactions, and the impulsive loads they induce, do not occur. The combined effect of the flight trajectory and the aerodynamic interaction between the main and tail rotors is to induce a non-impulsive noise signature generated at a frequency of two-per-rotor revolution by the tail rotor in quartering flight. It should be noted, however, that the noise produced as a result of orthogonal blade-vortex interaction between the tail rotor blades and main rotor tip vortices is highly dependent on the relative vertical location of the tail rotor with respect to the main rotor. As a result, this mechanism is likely to become a larger contributor to the overall tail rotor noise when tail rotor is mounted at a lower location than that explored in the present work.

The impulsiveness of the noise generated by the tail rotor in high speed forward flight is increased when the discretisation used within the simulation is refined and thus the vortical structures within the wake and the distribution of blade loading over the tail rotor disc are resolved to finer scales. Furthermore, the level of sound predicted at frequencies well above the tail rotor blade passage frequency in quartering flight increases considerably when the resolution of the simulation is increased. These results indicate that whilst simulation at a higher resolution is a necessity in order to permit time-accurate comparisons against experimental measurements of sound pressure at fixed ob-
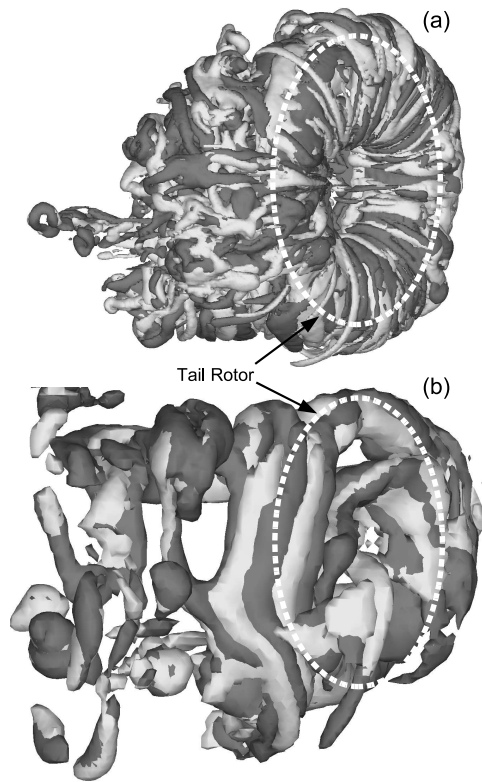
server locations, the principal sources of tail rotor noise can be understood using the efficient approach to modelling the aerodynamics of the rotor blades and the evolution of the rotor wake used here.

References

[1]Sheridan, P.F., and Smith, R.P. Interactional Aerodynamics – A New Challenge to Helicopter Technology, *Journal of the American Helicopter Society*, 1980, **25**, (1), pp. 3–21.

[2]Leverton, J.W., Pollard, J.S, and Wills, C.R. Main Rotor Wake/Tail Rotor Interaction, *Vertica*, 1977, **1**, (3), pp. 213–221.

[3]Leverton, J.W., and Pike, T.C., The Importance of Tail Rotor Interaction as an Acoustic Source, *Proceedings of the 49th American Helicopter Society Annual Forum*, St. Louis, Missouri, USA, 19–21st May 1993.

[4]Leverton, J.W. EH101 Advanced Technology Rotorcraft: Design for Low Noise, *Applied Acoustics*, **32**, (1), 1991, pp. 13–22.

[5]Schultz, K.J., and Splettstoesser, W.R. Helicopter Main Rotor/Tail Rotor Noise Radiation Characteristics from Scaled Model Rotor Experiments in the DNW, *Proceedings of the 49th American Helicopter Society Annual Forum*, St. Louis, Missouri, USA, 19–21st May 1993.

[6]Yin, J.P., Van der Wall, B., and Oerlemans, S. Representative Test Results from HeliNOVI Aeroacoustic Main Rotor/Tail Rotor/Fuselage Test in DNW, *Proceedings of the 31st European Rotorcraft Forum*, Florence, Italy, 13–15th September 2005.

[7]Yin, J.P., Dummel, A., Falchero, D., Pidd, M., Prospathopoulos, J., Visingardi, A., and Voutsinas, S.G. Analysis of Tail Rotor Noise Reduction Benefits using HeliNOVI Aeroacoustic Main/Tail Rotor Test and Post-Test Prediction Results, *Proceedings of the 32nd European Rotorcraft Forum*, Maastricht, The Netherlands, 12–14th September 2006.

[8]Tadghighi, H. An Analytical Model for the Prediction of MR/TR Interaction Noise, *Proceedings of the 12th AIAA Aeroacoustics Conference*, San Antonio, Texas, 10–12th April 1989.

[9]Farassat, F., and Succi, G.P. The Prediction of Helicopter Rotor Discrete Frequency Noise, *Vertica*, 1983, **7**, (4), pp. 309–320.

[10]Yin, J.P., and Ahmed, S.R. Aerodynamics and Aeroacoustics of Helicopter Main-Rotor/Tail-Rotor Interaction, *Proceedings of the 5th AIAA/CEAS Aeroacoustics Conference and Exhibit*, Bellevue, Washington, 10–12th May 1999.

[11]Fletcher, T.M., and Brown, R.E. Main Rotor – Tail Rotor Interaction and Its Implications for Helicopter Directional Control, *Journal of the American Helicopter Society*, 2008, **53**, (2), pp. 125–138.

[12]Brown, R.E. Rotor Wake Modeling for Flight Dynamic Simulation of Helicopters, *AIAA Journal*, 2000, **38**, (1), pp. 57–63.

[13]Brown, R.E., and Line, A.J. Efficient High-Resolution Wake Modeling using the Vorticity Transport Equation, *AIAA Journal*, **43**, (7), 2005, pp. 1434–1443.

[14]Weissinger, J. The Lift Distribution of Swept-Back Wings, *NACA Technical Memorandum,* No. 1120, March 1947.

[15]Toro, E.F. A Weighted Average Flux Method for Hyperbolic Conservation Laws, *Proceedings of the Royal Society of London, Series A: Mathematical and Physical Sciences*, 1989, **423**, (1865), pp. 401–418.

[16]Kelly, M.E, Duraisamy, K., and Brown, R.E. Predicting Blade Vortex Interaction, Airloads and Acoustics using the Vorticity Transport Model, *Proceedings of the 9th American Helicopter Society Aeromechanics Specialists' Meeting*, Fisherman's Wharf, San Francisco, USA, 23–25th January 2008.

[17]Lynn, R.R., Robinson, F.D., Batra, N.N., and Duhon, J.M. Tail Rotor Design Part 1: Aerodynamics, *Journal of the American Helicopter Society*, 1970, **15**, (4), 1970, pp. 2–15.